Atmos. Chem. Phys., 17, 175–192, 2017
www.atmos-chem-phys.net/17/175/2017/
doi:10.5194/acp-17-175-2017

Atmospheric Chemistry and Physics
Open Access
EGU

New particle formation in the southern Aegean Sea during the Etesians: importance for CCN production and cloud droplet number

Panayiotis Kalkavouras[1], Elissavet Bossioli[1], Spiros Bezantakos[2], Aikaterini Bougiatioti[3,7], Nikos Kalivitis[3], Iasonas Stavroulas[3], Giorgos Kouvarakis[3], Anna P. Protonotariou[1], Aggeliki Dandou[1], George Biskos[4,5], Nikolaos Mihalopoulos[3,5,6], Athanasios Nenes[6,7,8,9], and Maria Tombrou[1]

[1]Department of Physics, National and Kapodistrian University of Athens, Athens, 15784, Greece
[2]Department of Environment, Univ. of the Aegean, Mytilene 81100, Greece
[3]Env. Chemical Processes Lab., Dept. of Chemistry, Univ. of Crete, Heraklion 71003, Greece
[4]Fac. of Civil Engineering and Geosciences, Delft Univ. of Technology, Delft 2628 CN, the Netherlands
[5]Energy Environment and Water Research Center, The Cyprus Institute, Nicosia 2121, Cyprus
[6]Institute of Env. Research & Sustainable Development, National Observatory of Athens, Palea Penteli 15236, Greece
[7]School of Earth and Atmospheric Sciences, Georgia Institute of Technology, Atlanta, GA 30332, USA
[8]School of Chemical and Biomolecular Engineering, Georgia Institute of Technology, Atlanta, GA 30332, USA
[9]Institute for Chemical Engineering Science, Foundation for Research and Technology Hellas, Patra 26504, Greece

Correspondence to: Maria Tombrou (mtombrou@phys.uoa.gr)

Received: 15 April 2016 – Published in Atmos. Chem. Phys. Discuss.: 31 May 2016
Revised: 14 October 2016 – Accepted: 2 December 2016 – Published: 4 January 2017

Abstract. This study examines how new particle formation (NPF) in the eastern Mediterranean in summer affects CCN (cloud condensation nuclei) concentrations and cloud droplet formation. For this, the concentration and size distribution of submicron aerosol particles, along with the concentration of trace gases and meteorological variables, were studied over the central (Santorini) and southern Aegean Sea (Finokalia, Crete) from 15 to 28 July 2013, a period that includes Etesian events and moderate northern surface winds. Particle nucleation bursts were recorded during the Etesian flow at both stations, with those observed at Santorini reaching up to 1.5×10^4 particles cm^{-3}; the fraction of nucleation-mode particles over Crete was relatively diminished, but a higher number of Aitken-mode particles were observed as a result of aging. Aerosol and photochemical pollutants covaried throughout the measurement period; lower concentrations were observed during the period of Etesian flow (e.g., 43–70 ppbv for ozone and 1.5–5.7 $\mu g\, m^{-3}$ for sulfate) but were substantially enhanced during the period of moderate surface winds (i.e., increase of up to 32 for ozone and 140 % for sulfate). We find that NPF can double CCN number (at 0.1 % supersaturation), but the resulting strong competition for water vapor in cloudy updrafts decreases maximum supersaturation by 14 % and augments the potential droplet number only by 12 %. Therefore, although NPF events may strongly elevate CCN numbers, the relative impacts on cloud droplet number (compared to pre-event levels) is eventually limited by water vapor availability and depends on the prevailing cloud formation dynamics and the aerosol levels associated with the background of the region.

1 Introduction

During summer and early autumn (warm period), the circulation over the eastern Mediterranean (EM) is dominated by a persistent northerly flow known as the Etesians (Tyrlis and Lelieveld, 2013). Under the prevalence of the Etesians, the advection of the air masses is pronounced over the EM, rendering the atmospheric conditions as the most important factor for high concentrations of gases and aerosol particles even in remote areas. The scientific interest in the Aegean

Sea (AS), which is part of the EM, has led to a number of experimental campaigns during the warm period (Mihalopoulos et al., 1997; Paronis et al., 1998; Formenti et al., 2002a, b; Kouvarakis et al., 2002; Lelieveld et al., 2002; Zerefos et al., 2002), focusing initially on the interpretation of ozone (O_3) enhancement under the Etesian regime. Apart from the simultaneous contribution of local and distant sources in the area, in the presence of enhanced photochemistry, strong subsidence was also identified in most of these events (Kallos et al., 1998, 2007; Lelieveld et al., 2002; Salisbury et al., 2003; Kalabokas et al., 2007, 2008, 2013; Kanakidou et al., 2011; Bossioli et al., 2016). Airborne measurements performed during an Etesian outbreak (Aegean-GAME campaign; Tombrou et al., 2015) clearly showed that neutral to stable atmospheric conditions prevailed over the northern and central AS, with reduced friction velocities and absolute turbulent fluxes (momentum or heat) cumulating the concentrations below the planetary boundary layer (PBL) and mainly inside the shallow marine atmospheric boundary layer (MABL). Unstable conditions were found only over the southeastern AS, in the vicinity of Crete, resulting in enhanced friction velocities and large positive values of sensible heat flux.

Long-term aerosol observational studies in the EM have relied on ground measurements collected at Finokalia, a remote coastal site in the northeast of Crete (Bardouki et al., 2003; Eleftheriadis et al., 2006; Lazaridis et al., 2006; Gerasopoulos et al., 2007; Kalivitis et al., 2008, 2014, 2015; Koulouri et al., 2008; Querol et al., 2009; Pikridas et al., 2010, 2012), and a few more at the Akrotiri station on western Crete (Lazaridis et al., 2008; Kopanakis et al., 2012, 2013). Most of these ground-based observations indicate that the mass of fine aerosols presents a summer maximum; however, their appearance is season independent. These fine aerosols have been related to regional sources of pollution enhanced by long-range transport during the Etesian flow. In particular, a mixture of anthropogenic (Koçak et al., 2011), biogenic (Im and Kanakidou, 2012), and biomass burning emissions (Sciare et al., 2008; Bougiatioti et al., 2014), originating mainly from the Balkans and central and eastern Europe, result in enhanced aerosol concentrations in the southern AS (Kalivitis et al., 2014).

A few short-lived particle formation events (18–25 nm) were first recorded at Finokalia by Kalivitis et al. (2008), arriving with low speed from the west during autumn. Thereafter, new particle formation (NPF) events have been frequently observed at Finokalia (Manninen et al., 2010; Ždímal et al., 2011; Pikridas et al., 2012; Kalivitis et al., 2014, 2015) and Akrotiri (Kopanakis et al., 2013) throughout different periods of the year, but more frequently during winter. NPF events are favored when air masses are enriched by a reactant (e.g., NH_3) prior to reaching the site at Finokalia (Pikridas et al., 2012; Kalivitis et al., 2014). During Etesian flow conditions, the particle size distributions were centered at the lower end of the accumulation-mode size range (Kalivitis et al., 2014). This was partly attributed to the production of sufficient sulfuric acid to increase the condensation sink and suppress NPF events during the summer (Pikridas et al., 2012). It has been only recently shown that NPF events could occur at Finokalia during Etesians (Kalivitis et al., 2015). A large number of PM_1 particles (of the order of $10^4\,cm^{-3}$) were also observed in the northeastern AS during an Etesian outbreak (Tombrou et al., 2015), whereas high number concentrations of nucleation-mode particles observed in the northern AS by Triantafyllou et al. (2016) have been associated with polluted air masses transported from Istanbul.

The above drives the need to understand the history of the air masses as they transect the Aegean before arriving at Finokalia. In particular, we need to elucidate the atmospheric and chemical processes that affect aging of the air masses passing over the AS maritime area between the Cyclades and Crete. Furthermore, we need to examine whether NPF events observed at Finokalia would be stronger over the central Aegean during the northern Etesian flow. Bougiatioti et al. (2009, 2011) observed high cloud condensation nuclei (CCN) concentrations at Finokalia from air masses coming from the Balkans during a period representative of an Etesian regime, while Kalivitis et al. (2015) recently demonstrated that the NPF events are associated with an increase in the concentration of CCN production in the EM atmosphere. However, few studies to date have focused on understanding the increase in cloud droplet number that results from NPF, which is the true microphysical link between NPF and the aerosol indirect effect.

Driven by the arguments above, we chose to perform measurements at a remote site on Santorini, which is located within the same path of air masses that reach the station of Finokalia during the Etesians. Our aim is to elucidate both atmospheric and chemical processes that affect aging of the air masses passing over the AS before reaching its southern edge, the island of Crete. Continuous ground measurements of particle properties, concentration of gaseous species, and meteorological variables were simultaneously collected on Santorini and Crete. During this short-term campaign (15–28 July 2013) intense bursts of nucleation-mode particles were observed at both sites. The synoptic wind flow and boundary layer dynamics, as well as the atmospheric chemical composition that favor the enhanced NPF events during the Etesian flow, are examined in this study. To understand how NPF could affect cloud formation, we quantify its impact on CCN levels, cloud droplet number concentration (CDNC), and supersaturation formed in clouds that develop before, during, and after NPF events at both ground sites. Complementary to this analysis, wind patterns and atmospheric chemical composition based on WRF-Chem (Grell et al., 2005) mesoscale model simulations are presented.

Table 1. Summary of the variables and operation characteristics of the instruments at Santorini and Finokalia stations.

Santorini	Instrument	Resolution	Period of operation
Aerosols			
Aerosol number distribution (10–500 nm)	TSI 3034 SMPS	3 min	15–28 July
Gaseous species			
O_3	M400E photometric ozone analyzer	1 min	18–28 July
SO_2	M100E UV fluorescence analyzer	1 min	15–28 July
NO, NO_2, NO_x	M200E nitrogen oxide analyzer	1 min	15–28 July
Finokalia			
Aerosols			
Aerosol number distribution (9–848 nm)	TROPOS type SMPS	5 min	16–29 July
Chemical composition (SO_4^{2-}, NO_3^-, NH_4^+, Cl^-, organics)	Aerodyne Research Inc. aerosol chemical speciation monitor (ACSM)	30 min	15–28 July
Gaseous species			
O_3	Thermo electron Model 49i	3 min	15–28 July
Meteorology			
Relative humidity, temperature	MP101A humidity-temperature	5 min	15–28 July
Wind speed, direction	05103 wind monitor	5 min	15–28 July

2 Methodology

2.1 Experimental observations

Ground-level measurements were conducted simultaneously at two remote coastal areas (see Fig. 1) from 15 to 28 July 2013: on the island of Santorini (at Ag. Artemios, 36°26′ N, 25°26′ E) and at the monitoring station of Finokalia on the island of Crete (35°20′ N, 25°40′ E; http://finokalia.chemistry.uoc.gr; Mihalopoulos et al., 1997). Ag. Artemios (hereafter referred to as Santorini) is located at an elevation of 153 m above sea level (a.s.l.), while Finokalia is located on the top of a hill at 260 m a.s.l. Both measuring sites are far from any large city or anthropogenic activity and are close to the sea; Finokalia faces the sea within a sector of 270 to 90°, whereas the station on Santorini faces the sea within a sector of 340 to 120°.

The Finokalia station houses a suite of instruments for measuring the meteorological parameters, the concentrations of gaseous species, and the physical properties and chemical composition of atmospheric particles. We used an O_3 analyzer (Thermo Electron model 49I), a scanning mobility particle sizer (SMPS, TROPOS type; Wiedensohler et al., 2012) with a TSI-3772 condensation particle counter (CPC) for measuring the size distribution of aerosol particles with diameters from 9 to 848 nm (scanned range), and an Aerodyne Research Inc. aerosol chemical speciation monitor (ACSM; Ng et al., 2011) for measuring the mass and chemical composition (SO_4^{2-}, NO_3^-, NH_4^+, Cl^-, and organics) of non-refractory submicron aerosol particles. A TSI SMPS (Model 3034) measured the size distribution of particles with diameters from 10 to ca. 500 nm at Santorini. The concentrations of gaseous species were also measured using an O_3 analyzer (Photometric M400E), a dual channel chemiluminescence analyzer for nitrogen oxides (NO, NO_2; Photometric M200E), and a fluorescence analyzer for sulfur dioxide (SO_2; Photometric M100E). An overview of the instruments used for the measurements is provided in Table 1.

2.2 CCN and droplet number calculations

CCN concentrations are calculated using the observations of size distribution and chemical composition as follows. First, Köhler theory (Köhler, 1936; Seinfeld and Pandis, 2006; Petters and Kreidenweis, 2007) is applied to determine, based on knowledge of aerosol composition, the minimum dry size of

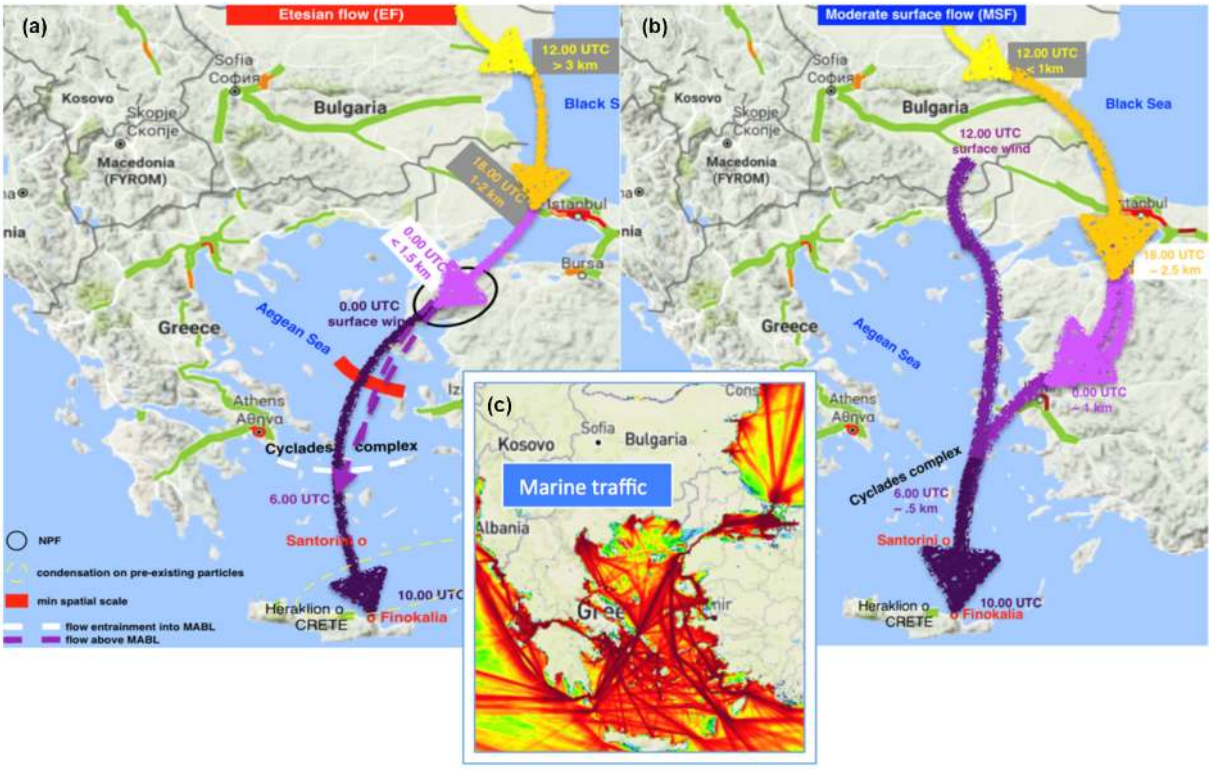

Figure 1. The extended area of study where the major routes (arrows) of air masses pass through Santorini and Finokalia on 23 July (EF – left panel) and 26 July (MSF – right panel) is indicated. In the left panel, the areas of NPF (black ellipse), the spatial extent of NPF event (red line), flow entrainment into MABL (white dashed line), and the condensation (yellow dashed ellipse) are shown. The major traffic (green) and urban (red) emission sources are also shown. The marine traffic is shown in the middle panel.

particles, d_c, that can activate at a given level of supersaturation, s. Then, the CCN concentration is determined from the observed size distributions by calculating the concentration of particles with sizes above d_c (Seinfeld and Pandis, 2006). s is either prescribed or determined from a cloud parameterization, both of which are performed here. Chemical composition is expressed in terms of the hygroscopicity parameter, κ, (Petters and Kreidenweis, 2007).

Thereafter, we calculate the droplet number (N_d) and supersaturation for clouds forming in the vicinity of both sites during all NPF events. The droplet parameterization used is based on the "population splitting concept" of Nenes and Seinfeld (2003), later improved by Barahona et al. (2010) and Morales Betancourt and Nenes (2014). In the calculations of droplet number, the size distribution is represented by the sectional approach, derived directly from the SMPS distribution files. The updraft velocity was calculated from high-resolution airborne measurements performed over this region of AS under similar atmospheric conditions (Tombrou et al., 2015). The partial sensitivity of cloud droplet number to chemical composition and vertical velocity is derived from the finite difference approach (Karydis et al., 2012).

2.3 Regional modeling

The WRF-Chem version 3.3 mesoscale model (Grell et al., 2005) is used to understand the dominant meteorological regimes and the regional characteristics of the aerosols during the sampling period. Simulations were performed by applying two-way nesting with three domains: the outermost first domain covers the extended area of Europe (spatial resolution $0.5° \times 0.5°$), the second domain covers the extended area of Greece and Italy ($0.167° \times 0.167°$), and the innermost third domain is centered on the extended area of Greece ($0.056° \times 0.056°$).

The RADM2 chemical mechanism is used to simulate the gas-phase chemistry (Stockwell et al., 1990). Aerosol dynamics are treated with the Modal Aerosol Dynamics Model for Europe (MADE; Ackermann et al., 1998). Aerosols in MADE are represented by two lognormal size distributions that correspond to the Aitken and accumulation modes. Supermicrometer particles are represented by a coarse mode (Schell et al., 2001). NPF in MADE is treated with the Kulmala et al. (1998) parameterization of sulfuric acid nucleation, although it is now well-documented that other reagents (e.g., NH_3 and organics) play important roles in this process (Kulmala et al., 2004). New particles with a diame-

ter of 3.5 nm, are assigned to the Aitken mode and the size distribution parameters are adjusted to retain the lognormal shape of the distribution. Condensation rates of low-vapor-pressure gas-phase species onto existing particles are determined by Binkowski and Shankar (1995). The secondary organic aerosol (SOA) model (SORGAM; Schell et al., 2001) is used to simulate organic aerosol. The aerosol species treated by the modules are the main inorganic ions (SO_4^{2-}, NO_3^-, NH_4^+, Na^+, Cl^-), elemental carbon (EC), primary organic aerosols (POA), SOA, a primary unspeciated $PM_{2.5}$ fraction covering all the unspeciated and/or unknown fine particles ($PM_{2.5\text{-unsp}}$), and three species for the coarse mode (i.e., anthropogenic, marine, and soil-derived aerosols). For the fine particle fraction, each model species has an Aitken mode and an accumulation mode. The lack of a dedicated nucleation mode in the model neglects the actual processes of particle formation and growth towards the Aitken mode and eventually leads to unrealistic lifetimes against deposition and coagulation as well as to unrealistic growth rates. In the framework of this study we use the results of WRF-Chem mainly to investigate the flow advection and chemical composition.

For anthropogenic emissions from Europe (first and second domains) we use the EMEP database (http://www.ceip.at/webdab-emission-database), while for Greece (third domain) we employ the national emission inventory (Tombrou et al., 2009). Natural (biogenic and sea-salt) emissions are calculated online within the WRF-Chem model. Biomass burning emissions are not considered. The chemical boundary conditions used in this study are based on an idealized, northern hemispheric, mid-latitude, clean environmental vertical profile from the NOAA Aeronomy Lab Regional Oxidant Model (NALROM; Liu et al., 1996; Peckham et al., 2011). Simulations were performed from 12 to 29 July. An extended evaluation of the WRF-Chem model against airborne and ground observations over the AS during the Etesians is presented in Bossioli et al. (2016). Under long-range transport conditions, the model successfully simulates CO, O_3, sulfate, and ammonium concentrations, while it underestimates the aerosol carbonaceous fraction, which is mostly organic matter. The biases were mainly attributed to underestimated POA emissions and limitation of the RADM2 mechanism regarding the treatment of monoterpene emissions (Tuccella et al., 2012).

Air mass origin and trajectories were determined by HYSPLIT4 (Hybrid Single-Particle Lagrangian Integrated Trajectory; www.arl.noaa.gov/ready/hysplit4.html) back-trajectory analysis (Stein et al., 2015). The back-trajectories, initialized with meteorological conditions from GDAS (0.5°), were computed at several heights. All three-dimensional trajectories were computed with an end point either at the Santorini or Finokalia station.

3 Results and discussion

3.1 Prevailing atmospheric and air quality conditions

Northern winds prevailed over the AS throughout the entire campaign. Based on the simulated wind patterns at 100 m above ground level (a.g.l.) throughout Greece (see Fig. S1 in the Supplement) and on the sea-level pressure fields (NCEP/NCAR; Fig. S2), 17–18 July and 22–24 July are periods of strong Etesian winds (Brody and Nestor, 1985; Kotroni et al., 2001; Anagnostopoulou et al., 2014). Hereafter, we refer only to the second period, as higher aerosol number concentrations were measured at both stations, but also because there were no O_3 measurements at Santorini, during the first period. Immediately after the second period, another characteristic period (25–27 July) with a similar pressure pattern to the previous two followed; the pressure gradient over the Dardanelles was weaker. Back-trajectory analysis of the air masses sampled at both stations indicates almost the same source regions for both periods (Figs. 2, S3). However, different conditions prevailed during these two periods, altering mainly the last part of the journey of the air masses over the AS. From 22 to 24 July, strong northern wind speeds prevailed ($> 10\,m\,s^{-1}$), with the wind direction forming the characteristic "ring shape" (Fig. S1) of the Etesian flow around Turkey (Tyrlis and Lelieveld, 2013). From 25 to 27 July, moderate surface wind speeds (up to ca. $8\,m\,s^{-1}$) with northeasterly surface flow were present over the central and southern AS, while stagnant conditions prevailed in the north (Figs. S1, S2). Hereafter, the two periods will be referred to as Etesian Flow (EF) and Moderate Surface Flow (MSF).

The measured wind speed at the Finokalia station exceeded $9\,m\,s^{-1}$, and the wind direction was mainly from the west-southwest during the daytime hours (Fig. 3) owing to topographic features that steer the prevailing direction towards the west-southwest direction. Capturing this local feature is a known challenge for regional models (e.g., Gauss et al., 2011; Im et al., 2011; Hodnebrog et al., 2012). At the same time, the simulated wind direction at the Santorini station exhibited a northern direction, with wind speeds exceeding $8\,m\,s^{-1}$ during the daytime hours (Fig. 3).

The number concentrations for the three particle modes (nucleation, Aitken, and accumulation), together with the O_3 concentrations, are shown in Fig. 4 for both periods at the Santorini and Finokalia stations. Simultaneous routine meteorological measurements, such as surface temperature and relative humidity, are also provided for each station. Apart from the region-wide differences, intense bursts in the concentration of nucleation-mode particles with diameters smaller than 25 nm were observed at both stations during the periods of EF (Fig. 4, shaded with yellow); it should be noted that these events were not observed at any of the stations during the period of MSF (Fig. 4, shaded with grey). In the subsequent sections the different characteristics and pro-

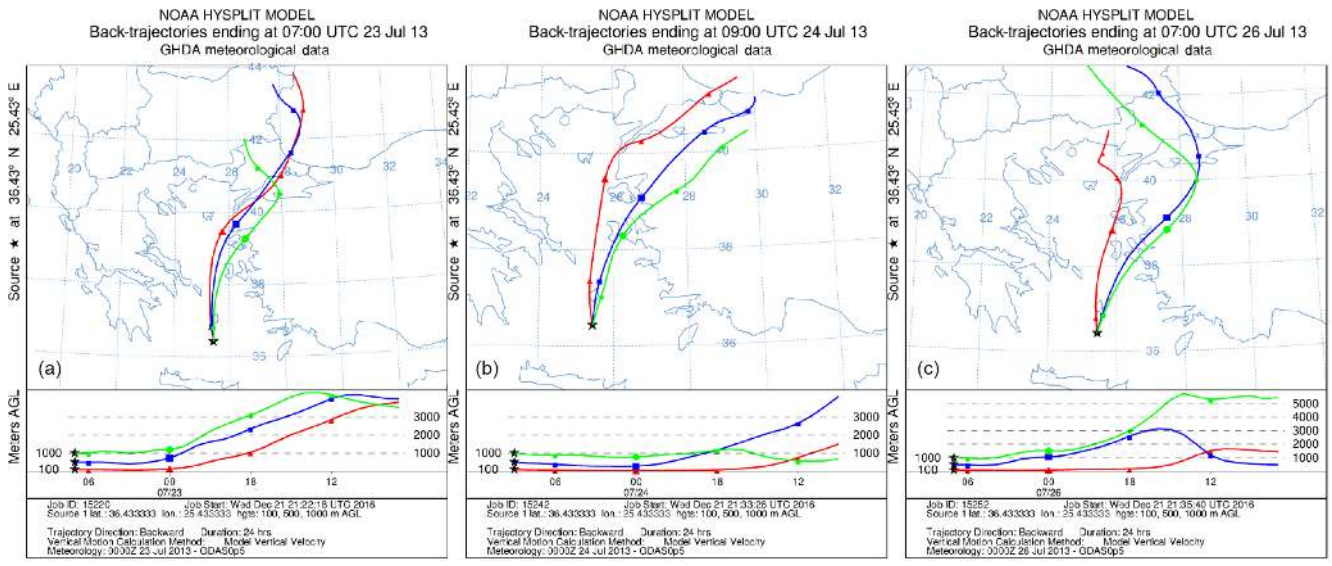

Figure 2. HYSPLIT4 back-trajectories computed with an end point at the Santorini station (from the heights of 100, 500, and 1000 m), on 23 (left panel), 24 (central panel) (both during EF period), and 26 July (MSF – right panel) 2013.

Table 2. Average (± standard deviation) of O_3 concentrations and aerosol mass and number concentrations during the two examined periods; (a) EF (22–24 July) and (b) MSF (25–27 July).

Tracer	Santorini	Finokalia	Santorini	Finokalia
	EF period		MSF period	
O_3 (ppbv)	51.4 ± 6.2	53.8 ± 4.5	70.0 ± 8.5	71.0 ± 7.9
Sulfate ($\mu g\,m^{-3}$)	N/A	3.1 ± 1.2	N/A	7.3 ± 1.5
Ammonium ($\mu g\,m^{-3}$)	N/A	1.4 ± 0.6	N/A	3.1 ± 0.6
Organics ($\mu g\,m^{-3}$)	N/A	4.2 ± 1.3	N/A	8.6 ± 1.2
Nitrate ($\mu g\,m^{-3}$)	N/A	0.38 ± 0.12	N/A	0.8 ± 0.1
Total number conc. (cm^{-3})	$3.6 \pm 2.1 \times 10^3$	$3.9 \pm 1.2 \times 10^3$	$2.0 \pm 0.6 \times 10^3$	$3.6 \pm 0.5 \times 10^3$
Aitken mode (cm^{-3})	$2.2 \pm 1.4 \times 10^3$	$2.5 \pm 1.5 \times 10^3$	$1.2 \pm 0.5 \times 10^3$	$1.6 \pm 0.5 \times 10^3$
Accumulation mode (cm^{-3})	$9.6 \pm 3.5 \times 10^2$	$1.6 \pm 0.9 \times 10^3$	$1.0 \pm 0.5 \times 10^3$	$2.1 \pm 0.6 \times 10^3$

cesses prevailing under EF or MSF are explored, aiming to elucidate the interconnection between the two stations.

3.2 Ozone concentrations

During the EF period, O_3 levels at the Santorini and Finokalia stations ranged between 38 and 66 ppbv and 43 to 70 ppbv, respectively (Figs. 4, S4; Table 2); these levels are consistent with previous measurements (57 ± 4 ppbv) inside the MABL for EF carried out during the Aegean-GAME campaign. The values also agree with the climatological values recorded over the greater area during summer (Gerasopoulos et al., 2005; Kalabokas et al., 2007, 2013). During EF, the less pronounced diurnal cycle at the Finokalia station (from 21 to 24 July the mean diurnal range is 8 ppbv; Fig. S4), compared to Santorini (18 ppbv; Fig. S4), is attributed to a shallower and more stable MABL over Santorini compared to Crete (Tombrou et al., 2015). This favors higher primary concentrations and thus O_3 scavenging at Santorini, especially when the MABL collapses during nighttime. In the vicinity of Crete, the MABL becomes less stable due to larger sea surface temperatures (SST) existing south of Santorini. This fact, together with the topography (i.e., Crete forms a mass of land that is located perpendicular to the EF), enhances the mixing and the downward transport from the layer above, which is rich in O_3 concentrations. During the MSF, high O_3 levels (the highest concentrations of the summer in 2013) were measured at both stations, ranging between 50 and 99 ppbv (Figs. 4, S4; Table 2). At both stations the highest values were observed on 26 July. The lower winds over the northern AS contributed to O_3 accumulation in this area, explaining the high O_3 concentrations at both stations. The maximum O_3 concentration observed (but simulated as well) at Finokalia had a 4 h delay compared to that observed at Santorini.

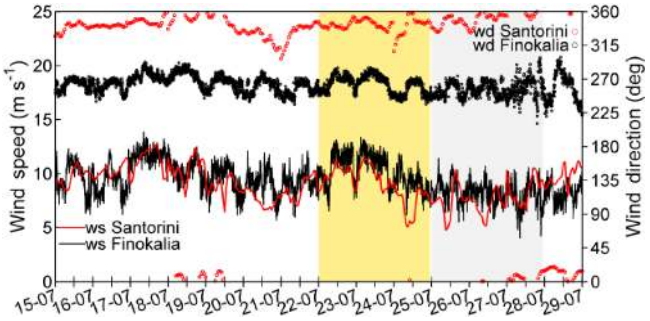

Figure 3. Time series of the wind speeds (ws, solid lines on left axis) and wind directions (wd, open circles, right axis) at Santorini (simulations from the WRF-Chem model) and at Finokalia (measurements). The second period of the EF is shaded with yellow and the MSF with grey.

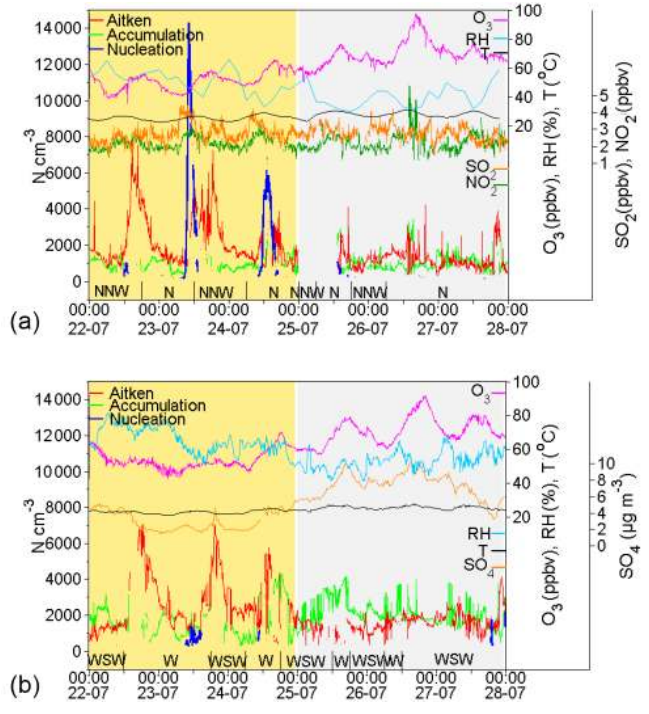

Figure 4. Aerosol modal number concentrations and pollutant (O_3, NO_2 when available) concentrations, along with meteorological parameters of relative humidity (RH) and surface temperature (T) at Santorini (top panel) and Finokalia (bottom panel). Note that SO_2 is shown at Santorini, while SO_4 is shown for Finokalia.

Simulations confirm that the air masses received at both stations during the prevailing strong northern wind are of the same origin, and they are representative of EF conditions (Fig. S3), albeit with an O_3 underprediction (average bias during afternoon hours up to −21 on 23 July and −15 % on 24 July, Figs. S4, 5). During the MSF period, simulations indicate an O_3 increase, especially in the southern AS, but it was also underpredicted (average bias during afternoon hours up to −24 % on 26 July, Figs. S4, 5). In case the chemical boundary conditions, including stratosphere–troposphere exchange processes, are represented realistically from a global chemical transport model, WRF-Chem simulates a significant O_3 increase inside the PBL (up to 40 %) during Etesians (Bossioli et al., 2016). Furthermore, inaccuracies of the emissions inventory could also have an impact on the results.

3.3 Aerosol mass and number concentrations

Figure 6 shows the non-refractory submicron aerosol concentrations measured at Finokalia during the whole experimental period. In general, the inorganic and organic mass concentrations behave similarly to O_3 (R^2 of O_3 to organics and inorganics is 0.5 and 0.59, respectively) during most of the experimental period (Figs. S4, 6). During EF, the PM_1 mass concentrations were reduced by roughly a factor of 2 compared to those during the MSF period (Table 2) and were in the range of concentrations measured in the framework of the Aegean-GAME campaign. However, despite that the concentrations of all four species (SO_4^{2-}, NO_3^-, NH_4^+ and organics) were substantially decreased during EF (23–24 July), the organic fraction exhibited a relative increase, especially at the beginning of this period. Due to lack of data at Santorini, simulated $PM_{2.5}$ mass concentrations were used for the analysis. The modeled concentrations for sulfate are about 2 μg m^{-3} at both stations at 09:00 LST (Fig. 7) quite close to the measured values at Finokalia (Fig. 6, on average during the EF they had an underprediction of 30 for sulfates and 60 % for ammonium). Similar to the case of O_3, the two stations are located along the less-polluted airflow over the AS.

During the MSF period, the aerosol mass concentrations at Finokalia were substantially higher (Table 2; Fig. 6). The increased concentrations were retained until noon of 27 July for sulfate and ammonium, while those of organics continued to increase further until the end of the campaign. The modeled spatial distribution of sulfate concentrations was nearly uniform over the AS, while similarly to O_3 the sulfate concentrations increased offshore of the northeastern coast of Crete due to the aging of air masses in combination with the strong impact of the topography (Fig. 7). The simulated mass concentrations of secondary inorganic fine aerosols also increased (simulated and observed concentrations correlate during both periods $R^2 = 0.8$); however, they are lower than the measured values at the Finokalia station (average underprediction of 50 for sulfates and 75 % for ammonium).

In contrast to the fine-aerosol mass concentrations, their total number concentrations were substantially increased, reaching continental levels during Etesian flow conditions (from 1.5×10^3 to 1.5×10^4 cm^{-3} at Santorini and from 2.4×10^3 to 7.5×10^3 cm^{-3} at Finokalia; Table 2, Fig. S5). The Aitken-mode particles followed a similar diurnal variation at both stations, ranging from 4.4×10^2 to 7.7×10^3 cm^{-3} and peaking around noon. Accumulation-mode particles were higher at Finokalia. The total particle

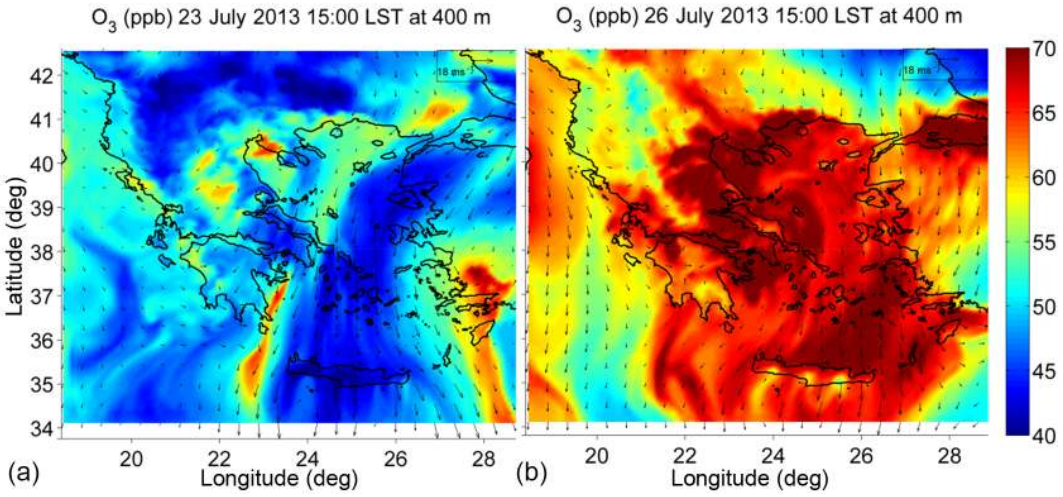

Figure 5. Spatial distribution of O_3 concentration (ppb) and wind speed ($m\,s^{-1}$; shown with arrows) at 400 m a.s.l. over the extended area of Greece as simulated by WRF-Chem at 15:00 LST for 23 July (EF – left panel) and 26 July (MSF – right panel).

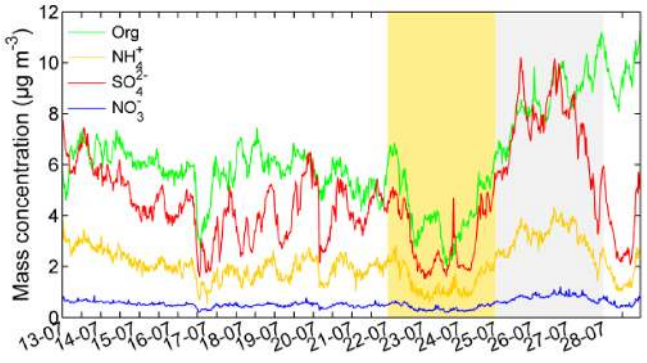

Figure 6. Mass concentrations of submicron aerosol measured at the Finokalia station from 13 to 30 of July 2013. The second period of the EF is shaded with yellow and the MSF with grey.

number concentrations measured within the MABL of the eastern AS during the Aegean-GAME campaign under similar atmospheric conditions were on average $8 \times 10^3\,cm^{-3}$, with almost 20 % ($1.4 \pm 1.2 \times 10^3\,cm^{-3}$) being in the 20–50 nm size range (Tombrou et al., 2015). Greater differences were observed for the nucleation-mode particles (i.e., particles with diameters smaller than 25 nm), with sudden concentration bursts observed at both stations (Fig. 4). On 23 July (EF), a nucleation-mode burst was recorded, reaching number concentrations of up to $1.3 \times 10^4\,cm^{-3}$ at Santorini and almost $1.4 \times 10^3\,cm^{-3}$ at Finokalia. A second event, but of lower intensity, was recorded on 24 July (EF). It is worth mentioning that apart from the strong winds and lower temperatures, this period is considered humid (relative humidity values reaching up to 80 % at the Finokalia station) in comparison to the MSF period (Fig. 4). The nucleation-mode particles shift gradually towards larger sizes in a banana-shape pattern at both stations, as shown in Fig. 8. The number of particles remained high for several hours at Santorini (see Fig. 8), indicating regional NPF (Kulmala et al., 2012).

The associated growth rates (GR) for particles that increased in size from 10 to 25 nm were estimated to be 3.06 at Santorini and $2.05\,nm\,h^{-1}$ at Finokalia on 23 July, and 2.08 and $1.76\,nm\,h^{-1}$, respectively, on 24 July. The average GR for particles increasing in size from 7 to 20 nm at Finokalia was reported by Pikridas et al. (2012) to be substantially higher ($7.5 \pm 5.8\,nm\,h^{-1}$), with the highest daily GRs observed during the hottest months of the year (May to July 2008). It should be mentioned, however, that the nucleation events reported in that study were mainly related to air masses spending most of the time over the island of Crete, which is not the case for the observations reported here. The formation rates of nucleation-mode particles, J_D, were computed according to Kulmala et al. (2012), considering both the coagulation flux and the condensational growth as sinks. For the two consequent events at Santorini, J_D for particles with diameters from 10 to 25 nm ranged between 4.82 (23 July, Fig. 8) and $2.77\,cm^{-3}\,s^{-1}$ (24 July, Fig. 8). At the station of Finokalia, J_D was lower for particles between 9 and 25 nm, ranging between 2.27 (23 July, Fig. 8) and $2.25\,cm^{-3}\,s^{-1}$ (24 July, Fig. 8). The similarity between the J_D rates at the two sites on 24 July indicates that a region-wide NPF event occurred, yet the rates taken a day earlier were markedly different, thus indicating a local event. However, we will show later (Sect. 3.4) that this was not the case and more information needs to be taken into account.

Under MSF conditions, the total fine-aerosol number concentrations were considerably lower than those during the EF (from 1.4×10^3 to 2.9×10^3 at Santorini and from 2.6×10^3 to $5.1 \times 10^3\,cm^{-3}$ at Finokalia, Fig. S5). Particles in the nucleation mode were absent, while the concentrations in the Aitken mode were substantially lower at both stations, vary-

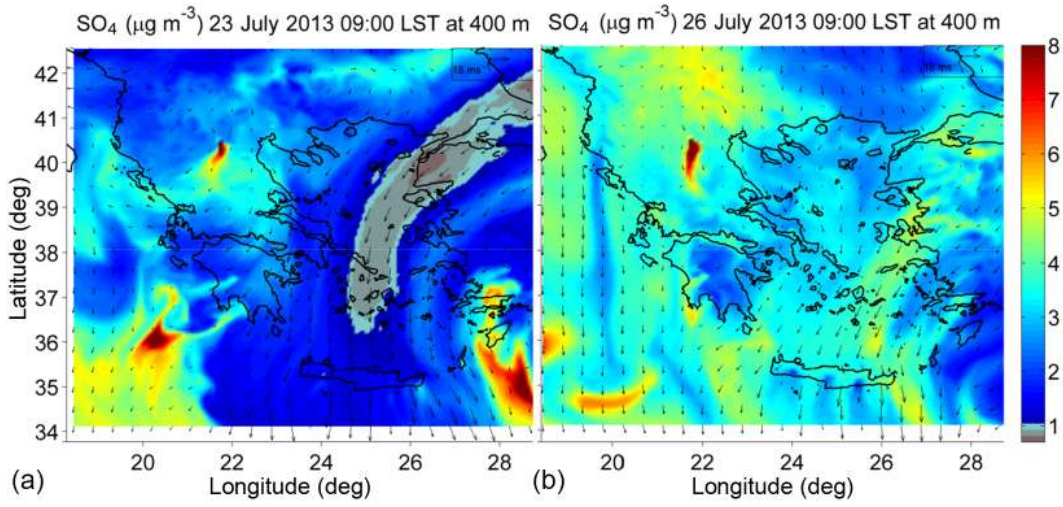

Figure 7. As in Fig. 5, but for sulfate concentration ($\mu g\,m^{-3}$) at 09:00 LST.

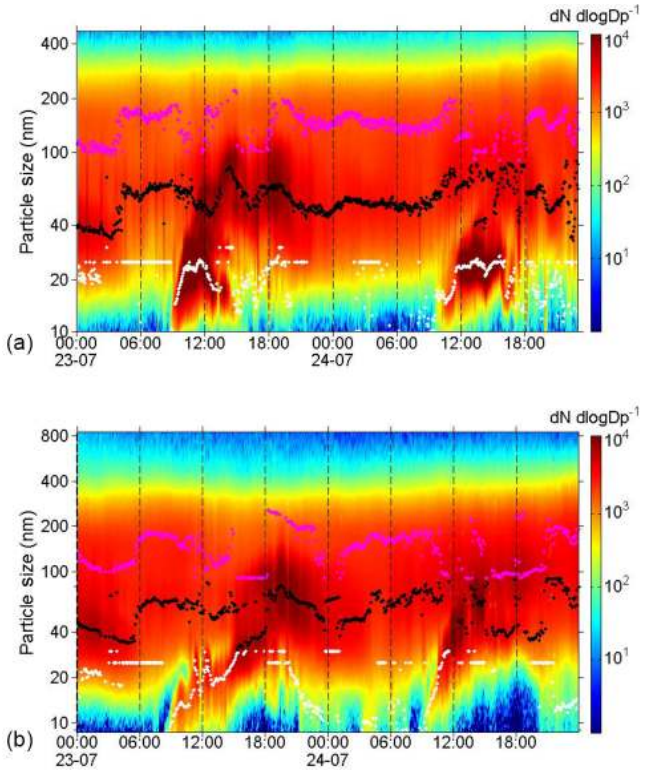

Figure 8. Diurnal evolution of the aerosol size distribution on 23 and 24 July (EF) at Santorini (top panel) and Finokalia (bottom panel). The white dots stand for nucleation, the black dots for Aitken, and the purple dots for accumulation geometric mean diameter.

ing from 3.2×10^2 to 4.1×10^3 cm^{-3} (Fig. S5). The particle concentrations in the accumulation mode at Santorini had a comparable variation to those of the Aitken mode, while they were apparently always higher at Finokalia.

3.4 Spatial extent of NPF event

The synoptic wind flow and boundary layer dynamics, as well as the chemical atmospheric background conditions that favor the enhanced NPF events during the EF, are further examined here. This type of event could be characterized as "type A" according to Boy and Kulmala (2002), owing to the sudden appearance of nucleation-mode particles and their consistent growth for at least 1 h. The horizontal scale of this event was estimated based on air mass back-trajectory analysis (Hussein et al., 2009), taking into account the time during which measurements at the site indicate a distinct nucleation mode. Following Birmili et al. (2003), HYSPLIT4 back-trajectory calculations started at the time when a nucleation mode was first distinguishable from the Aitken mode at Santorini and were performed for each subsequent hour until the two modes merged (nucleation duration). Following Crippa and Pryor (2013), the duration of NPF was based on the geometric mean diameter of particles, with sizes between 10 and 100 and from 30 to 100 nm; an event is said to initiate when the difference between the two geometric mean diameters becomes maximum and ends when this difference is less than 15 % (Fig. S6). Assuming a linear GR (Lehtinen and Kulmala, 2003), this approach showed that the ca. 10 nm particles (the smallest particles we could detect with our instrumentation) were able to grow up to 60 nm within 4.5 h of initial detection. This GR was then used to calculate the minimum spatial scale. On 23 July, the distance covered by the back trajectories within 4.5 h (starting when the nucleation-mode burst was first recorded at Santorini) spanned at least over 250 km to the northeast of Santorini in the center of AS, upwind of the Cyclades complex (Fig. 2; red line in Fig. 1, left panel). A couple of hours before the sunrise these back trajectories (both below and above 500 m a.g.l.) were observed over the northwestern Asian forest penin-

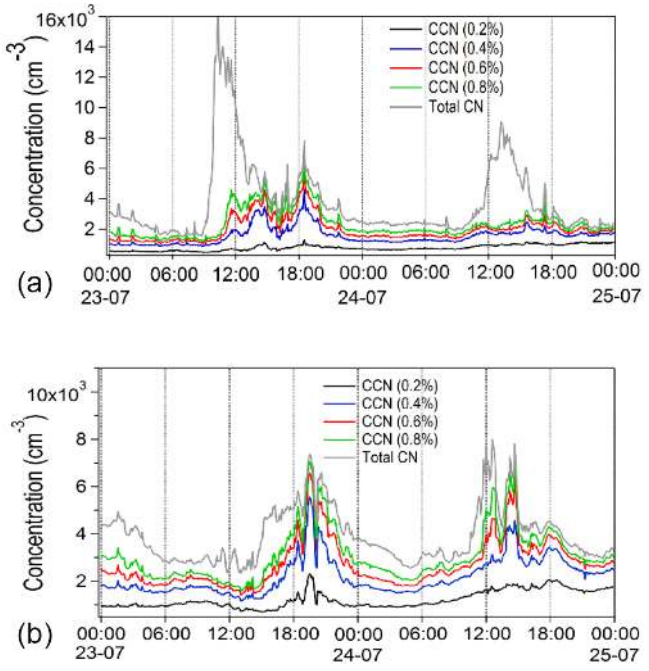

Figure 9. Time series of the CN and estimated CCN concentration particles for various supersaturations at Santorini (top panel) and Finokalia (bottom panel) on 23 and 24 July (EF). Time is in LST.

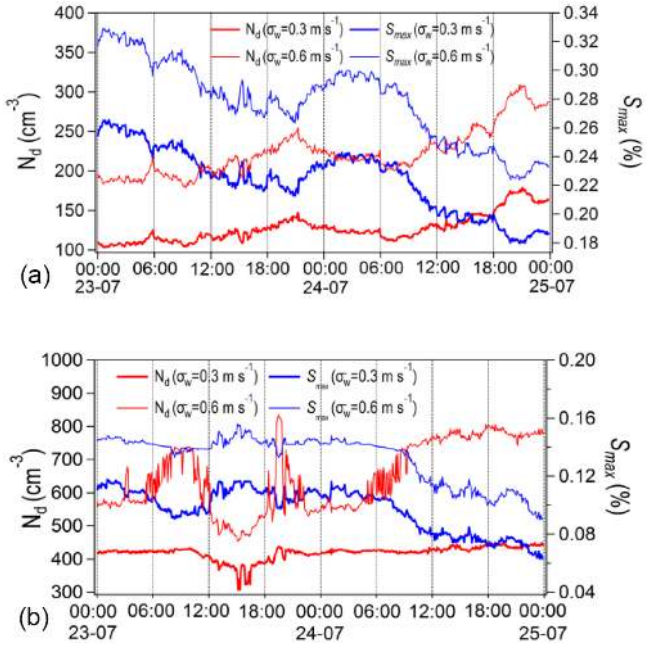

Figure 10. Time series of the estimated cloud droplet number concentrations (N_d, red lines) and maximum supersaturation in the cloud (s_{max}, blue lines) for updraft velocities (σ_w) of 0.3 m s^{-1} and 0.6 m s^{-1} at Santorini (top panel) and Finokalia (bottom panel) on 23 and 24 July (EF). Thick lines correspond to updraft velocity (σ_w) equal to 0.3 m s^{-1}, while thin lines correspond to 0.6 m s^{-1}.

sula of Turkey (area marked as black ellipse in Fig. 1, left panel; Fig. 2), having previously passed (at higher altitudes > 1.5 km a.g.l.) from the greater area of Istanbul (GAI) and the west coast of the Black Sea (from even higher altitudes > 3 km a.g.l.). A similar spatial extent also occurred during the less intense EF event on 24 July, although this started with a 2 h delay (Fig. 2). Air masses were better mixed throughout the boundary layer, covering a broader area over Asian Turkey on 24 July.

Despite the limitations of the model (absence of a nucleation mode, only binary homogeneous nucleation parameterization included), the conditions under which NPF events take place and their overall impact can still be estimated by conducting another simulation that deactivates the nucleation parameterization (nucleation-off run). According to the simulations, a wide stream of clean air masses of low preexisting aerosol particles (number concentrations $< 2.5 \times 10^3$ particles cm^{-3} not shown) but of sufficient H_2SO_4 ($\sim 10^7$ molecules cm^{-3} from high altitudes, not shown) overpasses the urban mixing height (at 1–2 km) over the GAI during the previous evening on 22 July (20:00 LST, Fig. 1, left panel), avoiding mixing with the local emissions. Thereafter, the air masses penetrated at lower levels (due to the EF structure) over northwestern Turkey (Fig. 2, left panel). In this forested area (black ellipse in Fig. 1, left panel) they find favorable conditions for NPF, such as low relative humidity, H_2SO_4, and availability of biogenic emissions (not shown) that further endorse the NPF efficiency. In Fig. S7, the number concentration of new particles (number concentration differences between nucleation-on and nucleation-off runs) at 1 km at 06:00 LST for both EF (left panel) and MSF (right panel) periods is presented. Although severely underestimated (simulated NPF contribution up to ~ 400 cm^{-3}), the critical role of the EF in the NPF event over the northern AS is revealed. Closer to the surface, the air masses had a substantial number of primary particles (emitted by the various activities of the GAI, Fig. S8), providing more surface available for condensation (NPF contribution up to 200 cm^{-3}, not shown). According to the simulations, a plume with large particulate load in the Aitken mode ($\sim 9 \times 10^3$ particles cm^{-3}) was transported over northwestern Turkey (Fig. S8, left panel). Our results agree with previous observations during an Etesian event, where number concentrations up to $\sim 1.2 \times 10^4$ cm^{-3} were observed in the northeastern AS, with the Aitken-mode particles dominating by up to 70 % (Tombrou et al., 2015). The less intense event on 24 July is associated with a narrow stream of low preexisting particles over the GAI (concentrations $< 2.5 \times 10^3$ particles cm^{-3}, not shown).

The plume, after crossing the Turkish mainland overnight, was transported over the AS, with most of the new particles above the stable MABL (Fig. S7, top-left panel; dashed purple lines in Fig. 1, left panel). The plume moved fast with rather negligible mixing, especially above the MABL,

thereby affecting areas located further away, such as the central AS, within a couple of hours after sunrise on 23 July (around 09:00 LST) and around noon on 24 July. The rapid advection above MABL, in combination with the low number of preexisting particles there (Fig. S7, bottom-left panel), seems to have left almost the majority of the newly formed particles intact. Thereafter, we mainly consider that while the part of the plume above the MABL passed over the Cyclades complex, the wakes on the lee side of the islands enhanced vertical mixing, enabling its entrainment into the MABL (area indicated with a white dashed line in Fig. 1, left panel). This assumption does not reject the fact that oxidation enhanced by photochemistry over the AS may also have contributed to the NPF process. The freshly nucleated particles that remained constantly inside the well-mixed MABL, suffered an early aging (i.e., growth by condensation and coagulation). The concentrations at both nucleation and Aitken modes jump almost simultaneously, accompanied by concurrent increases in O_3, NO_2, and SO_2 concentrations, at Santorini station during these two consequent events (Fig. 4). This could be an indication that this station receives masses simultaneously from different layers (inside and above the MABL), in line with a number of cases where maximum rate of change of ultrafine particle concentrations close to the surface was always preceded by breakdown of the nocturnal inversion and enhancement of vertical mixing (Crippa et al., 2012).

The air masses arrived 3 h later (after 13:00 LST; Fig. S3, left panel) at Finokalia on 23 July (Fig. 4). The 3 h transit timescale is in agreement with the prevailing wind speed (about $10\,m\,s^{-1}$; Fig. S1) and the 120 km distance between Santorini and Finokalia. The nucleation-mode particles were significantly reduced as they had shifted gradually towards larger sizes (Aitken mode) before reaching Finokalia (Fig. 4). The nucleated concentrations measured previously at Finokalia were probably due to a local nucleation event initiated at Heraklion (Crete). The current simultaneous measurements along the same flow stream show that both stations are under the influence of regional NPF events, during the Etesians.

During the MSF period on 26 July the air masses arriving at lower levels (below 500 m a.g.l.) at the Santorini station (Figs. 1, 2, both right panel) mainly passed from low altitudes over continental areas (< 1 km) and were substantially enriched by anthropogenic emissions, while those at higher levels covered longer distances over eastern Europe at the same time (exact opposite behavior of EF). Over the GAI, the simulated particle number concentration was much higher compared to EF conditions ($5–7 \times 10^3$ particles cm^{-3}, not shown), limiting the NPF event (Fig. S7). These atmospheric conditions promoted the mixing of air masses with local anthropogenic and natural emissions, favoring photochemical production of secondary pollutants such as O_3 (Fig. 5, right panel) and higher secondary aerosols (e.g., SO_4 shown in Fig. 7).

3.5 Impact of NPF events on CCN production

Understanding how NPF affects cloud formation requires quantification of its impact on the CCN levels that develop for cloud-relevant supersaturations. Since CCN concentrations were not measured, they were calculated using the observations of size distribution and chemical composition as already described in Sect. 2.2. The presentation of the results and the relevant discussion are based on the periods before and after the NPF events.

CCN concentrations are calculated for prescribed values of s between 0.2 and 0.8 %, corresponding to supersaturations found in relatively pristine stratiform to convective clouds (Seinfeld and Pandis, 2006). κ is calculated from the PM_1 chemical composition observed at Finokalia as follows: $\kappa = \varepsilon_{inorg}\kappa_{inorg} + \varepsilon_{org}\kappa_{org}$, where $\kappa_{inorg} = 0.6$ is the value for ammonium sulfate (Petters and Kreidenweis, 2007), and $\kappa_{org} = 0.16$ corresponds to the organic fraction (Bougiatioti et al., 2009), and ε_{inorg}, ε_{org} are the volume fractions of each constituent measured at Finokalia. The volume fractions range from 0.45 to 0.76 for inorganics and from 0.24 to 0.55 for organics, similar to the values measured under comparable atmospheric conditions from Bougiatioti et al. (2009, 2011) and Bezantakos et al. (2013). Throughout the measurement period, the aerosol-exhibited predicted values of hygroscopicity from 0.20 to 0.39, which is also consistent with the values determined by Bougiatioti et al. (2009, 2011) and Bezantakos et al. (2013). The aerosol hygroscopicity follows a diurnal cycle, being minimum just before noon and becoming maximum late in the afternoon, owing to a higher sulfate-to-organic-mass ratio (Fig. 6). Consequently, average κ values were estimated to be higher after the NPF events compared to the period before (increase by ~ 35 % on 23 July and up to 15 % on 24 July). Given a lack of PM_1 chemical composition measurements at Santorini, the chemical composition at Finokalia is applied instead to the Santorini size-distribution observations. The WRF simulations support this assumption because a similar chemical behavior is simulated for both stations (Figs. 5, 7). The model systematically underestimates the organic fraction at both stations (organic volume fraction does not exceed 0.2) but with minimal impact on resulting κ values since they do not differ from measurements for more than ± 6 % throughout the simulation period. From long-term measurements in the study area, the relative contribution of the main PM_1 constituents, including ammonium, is quite consistent over the years (Sciare et al., 2003; Koulouri et al., 2008; Bougiatioti et al., 2013). Thus, a sensitivity test of CCN concentrations to shifts in κ by ± 20 % is also carried out at Santorini.

The resulting CCN time series during Etesian flow are shown in Fig. 9. Average values of κ, d_c, and CCN concentrations at both stations before and after the NPF events are provided in Table 3. The calculated CCN number concentrations follow a diurnal cycle and tend to be at a maximum during the afternoon after the NPF events following the increase

Table 3. Average (± standard deviation) of calculated κ using the PM_1 chemical composition at Finokalia, the d_c (as described in the text), and the estimated CCN concentration particles at both stations on 23 and 24 July (EF period). Here s_{max} is the maximum supersaturation in the cloud, N_{total} is the total particle number concentration, and N_d is the potential cloud droplet number concentration calculated according to the approach described in the main text. Two probability density functions (PDFs) of the characteristic updraft velocity are used with $\sigma_w = 0.3\,m\,s^{-1}$ and $\sigma_w = 0.6\,m\,s^{-1}$. Time is in LST.

	Santorini		Finokalia		Santorini		Finokalia	
	23/7				24/7			
	Before 00:00–8:00	After 15:00–21:00	Before 00:00–10:00	After 17:00–21:00	Before 00:00–10:00	After 18:00–21:00	Before 00:00–11:00	After 17:00–21:00
κ	0.29 ± 0.01	0.36 ± 0.03	0.28 ± 0.02	0.38 ± 0.02	0.29 ± 0.01	0.34 ± 0.01	0.30 ± 0.01	0.34 ± 0.01
d_c (nm; $s = 0.2\,\%$)	104 ± 2	95 ± 2	104 ± 2	94 ± 1	101 ± 1	96 ± 1	102 ± 2	97 ± 1
d_c (nm; $s = 0.6\,\%$)	50 ± 1	46 ± 1	50 ± 1	45 ± 1	49 ± 1	46 ± 1	49 ± 1	46 ± 0
$CCN_{0.2}$ (cm^{-3})	536 ± 27	794 ± 145	1002 ± 76	1420 ± 383	682 ± 66	1028 ± 61	1062 ± 156	1822 ± 154
$CCN_{0.6}$ (cm^{-3})	1225 ± 90	3155 ± 789	2111 ± 196	4343 ± 1119	1535 ± 66	2004 ± 224	2191 ± 270	3346 ± 399
N_{total} (cm^{-3})	1777 ± 421	4621 ± 1986	3506 ± 699	5710 ± 779	2306 ± 154	2557 ± 351	3198 ± 384	3921 ± 404
$\sigma_w = 0.3\,m\,s^{-1}$								
s_{max} (%)	0.25	0.22	0.11	0.10	0.23	0.19	0.11	0.07
N_d (cm^{-3})	110 ± 4	124 ± 8	423 ± 4	407 ± 19	121 ± 5	165 ± 9	423 ± 3	440 ± 5
Activation Fr. (%)	6.5 ± 1.5	3.1 ± 1.1	12.5 ± 2.4	7.2 ± 0.6	6.4 ± 0.4	7.9 ± 1.2	13.4 ± 1.6	11.3 ± 1.1
Contribution of κ (%)	1.4	2.7	2.6	10.2	0.7	1.9	0.9	0.3
Contribution of N_{aer} (%)	98.6	97.3	97.4	89.8	99.3	98.1	99.1	99.7
$\sigma_w = 0.6\,m\,s^{-1}$								
s_{max} (%)	0.32 ± 0.01	0.28 ± 0.01	0.14 ± 0.01	0.14 ± 0.01	0.29 ± 0.01	0.23 ± 0.01	0.14 ± 0.01	0.11 ± 0.01
N_d (cm^{-3})	192 ± 6	217 ± 15	627 ± 67	619 ± 109	213 ± 7	286 ± 15	621 ± 73	786 ± 11
Activation Fr. (%)	11.4 ± 2.6	5.4 ± 1.9	18.8 ± 5.1	10.8 ± 0.7	11.3 ± 0.7	13.7 ± 2.1	19.7 ± 3.1	20.2 ± 1.9
Contribution of κ (%)	1.2	1.9	3.8	19.0	0.6	1.6	0.7	0.2
Contribution of N_{aer} (%)	98.8	98.1	96.2	81.0	99.4	98.4	99.3	99.8

of κ values. Most particles are CCN-active for $s \geq 0.6\,\%$, as they converge towards the total CN time series. Bougiatioti et al. (2009) observed similar behavior at Finokalia for polluted air masses with a similar origin (Balkans). For $s = 0.6\,\%$, d_c varied from 43 to 51 nm and CCN concentrations reached up to $\sim 6 \times 10^3\,cm^{-3}$ following the Aitken-mode concentrations at both stations (Figs. 4, 9). The higher CCN number concentrations at Finokalia, compared to those observed at Santorini (Table 3), were the result of a higher number of accumulation-mode particles passing previously from Santorini (that were too small to be CCN at Santorini, but grew to CCN-relevant sizes by the time they arrived at Finokalia, Sect. 3.3). Accordingly, the higher activation fractions (CCN / CN) were observed at the station of Finokalia with larger and more aged aerosol particles, while at Santorini this was observed at the end of the events, when the smaller particles dropped in concentration because they grew to larger sizes. On 23 July, the NPF event increased the CCN concentrations by 157 % at Santorini and 106 % at Finokalia, compared to their pre-event values. In some moments the increase reached up to a factor of 6. During the second less intense event on 24 July, the CCN increase was lower at both stations (31 % at Santorini and 53 % at Finokalia). The lower increase was also due to the pre-event background, characterized by higher CCN concentrations. Throughout the MSF period, the CCN concentrations decreased by almost 48 and 23 % at Santorini and Finokalia, respectively, compared to the levels during the NPF events. Changes in chemical composition, as described above, exhibit a relatively low variation in CCN concentrations (at $s = 0.6\,\%$) up to 10 %, following the same diurnal behavior. As expected, lowering the supersaturation at 0.2 % leads to the activation of larger particles, with d_c ranging from 91 to 106 nm, which is consistent with the observations reported by Kalivitis et al. (2015). At $s = 0.2\,\%$, both NPF events contribute up to 50 % to the increase of the CCN concentrations at both stations. However, the higher CCN production at Finokalia on 24 July is associated with the accumulation-mode particles at the end of both events.

3.6 Impact of NPF events on droplet number

Studying the impact of NPF on CCN concentrations at prescribed levels of supersaturation is a simple and frequently used approach for observational studies of NPF (e.g., Kalivitis et al., 2015 and references therein). However, it provides an incomplete description of NPF impacts on cloud droplet number because it does not consider the feedback of CCN on cloud supersaturation that develops in cloudy updrafts. Mechanistic cloud droplet formation parameterizations (Ghan et al., 2011; Morales Betancourt and Nenes,

2014) can capture this complexity by efficiently calculating the maximum supersaturation (s_{max}) that forms in a cloud given knowledge of the aerosol size distribution, composition, and updraft velocity. Observations suggest that the distribution of vertical velocities in the boundary layer displays a spectral dispersion of $\sigma_w = 0.2$–$0.3\,m\,s^{-1}$ around a zero average value, which is consistent with vertical velocities observed in marine boundary layers (e.g., Meskhidze et al., 2005; Ghan et al., 2011). When applying the droplet parameterization, we employed the "characteristic velocity" approach of Morales and Nenes (2010) to obtain velocity PDF-averaged values of CDNC and s_{max}. As a sensitivity test, we also considered calculations for a convective boundary layer ($\sigma_w = 0.6\,m\,s^{-1}$).

The calculation of PDF-averaged values of N_d and s_{max} was carried out for every distribution of aerosol number and composition measured for all NPF events. The resulting time series are shown in Fig. 10 for Santorini (top panel) and Finokalia (bottom panel). s_{max} is negatively correlated with N_d at both stations, owing to the increased competition for water vapor by the growing droplets when CCN increase. As a result, N_d responds sublinearly to CCN increases – the degree to which this occurs depends on the level of aerosol concentrations before and during the NPF event. At Santorini, the CCN levels are much lower than at Finokalia (Table 3); therefore, we expect the relative increase in N_d from NPF to be higher there. Assuming $\sigma_w = 0.3\,m\,s^{-1}$, the NPF events are associated with s_{max} decreases at both stations, compared to the period before the events. On 23 July, the decrease was on average 12 % at Santorini and 9 % at Finokalia. As a result, N_d concentrations during the NPF event increased by 13 % to $124 \pm 8\,cm^{-3}$ at Santorini, compared to the period before the event. At Finokalia, however, aerosol levels were much higher and N_d remained virtually the same before and after the NPF event (Table 3). The effect of the less intense NPF event on 24 July was higher; N_d concentration increased by 36 % at Santorini and 4 % at Finokalia compared to pre-event values. The decrease of s_{max} was also higher on this day, 17 % at Santorini and 36.4 % (at 0.06–0.08 %) at Finokalia (Table 3), owing to the higher accumulation-particle concentrations compared to the previous events. The variance of N_d during the event period, for σ_w equal to $0.3\,m\,s^{-1}$, was $475\,cm^{-3}$ at Santorini and $37\,cm^{-3}$ at Finokalia, while for σ_w equal to $0.6\,m\,s^{-1}$, the variance was 865 and $20\,cm^{-3}$, respectively. Altogether, this clearly shows that when NPF particles age (e.g., arrive at Finokalia) their competition for water vapor can reduce cloud supersaturation to very low levels.

The larger updraft velocity ends in larger values of s_{max}, which allow smaller particles to activate into cloud droplets. In particular, N_d exhibits a substantial increase for $\sigma_w = 0.6\,m\,s^{-1}$, but with a similar pattern to that with the lower velocity, especially at Santorini. This indicates that the impact of mean vertical velocity on the CDNC is higher at this station. In this case, the average N_d concentration was 217 ± 15 at Santorini and $619 \pm 109\,cm^{-3}$ at Finokalia (increase relative to $\sigma_w = 0.3\,m\,s^{-1}$ by 75 and 52 %) after the event on 23 July and 286 ± 15 and $786 \pm 11\,cm^{-3}$, respectively (increase relative to $\sigma_w = 0.3\,m\,s^{-1}$ by ~ 76 % for both stations) on 24 July. It is interesting to note that for $\sigma_w = 0.6\,m\,s^{-1}$ two N_d peaks were observed at Finokalia, of which the first is attributed to local processes since it was observed much earlier than the NPF event at Santorini. The stronger variation in N_d at Finokalia under the higher vertical wind compared to Santorini, indicates that vertical velocity variations likely dominate the variance of droplet number for clouds in the region of Finokalia. Furthermore, from the partial sensitivity of N_d to the total aerosol number and to κ, the relative contribution of chemical composition and total aerosol number to the variance of N_d is attributed. We find that in most cases the predicted N_d variability is almost exclusively governed by the aerosol number variation (> 98 %, Table 3) and to a lesser extent by the chemical composition (< 2 %). The relative contribution of chemical composition became more significant at Finokalia only after the intense NPF event on 23 July (10 % for $\sigma_w = 0.3\,m\,s^{-1}$ and 19 % for $\sigma_w = 0.6\,m\,s^{-1}$). This can be attributed to the more "aged" nature of the sampled aerosol at Finokalia, compared to the one at Santorini. This is consistent with the lower s_{max} predicted for Finokalia, leading to the activation of larger particle sizes that were subject to longer atmospheric processing during their transition to more unstable conditions after Santorini. Altogether, although NPF events may strongly elevate CCN numbers, the relative impacts on cloud droplet number (compared to pre-event levels) are eventually limited by water vapor availability and depend on the aerosol levels associated with the background.

4 Conclusions

Concentrations of chemically and size-resolved submicron aerosol particles along with concentrations of trace gases and meteorological variables were simultaneously measured at Santorini (central AS) and Finokalia on Crete (southern AS) from 15 to 28 July 2013. Two well-distinguished periods are identified: the first with strong wind speeds and wind directions forming the characteristic "ring-shape" of the Etesian flow (EF) around Turkey, and the second with moderate surface wind speeds and northerly direction over the AS (MSF). The two periods exhibited intense differences in air quality levels.

During EF, the mass concentrations were reduced by roughly a factor of 2 compared to those during the MSF period. The total number concentration of aerosol particles increased during the EF, varying from 1.5×10^3 to 1.5×10^4 at Santorini and from 2.4×10^3 to 7.5×10^3 particles cm^{-3} at Finokalia. Furthermore, intense bursts of nucleation-mode particles were recorded at both stations, with more intense bursts observed at Santorini. At Finokalia, the fragment of

nucleated particles was diminished and a higher number concentration of the Aitken-mode particles was observed, which was attributed to atmospheric mixing, growth process, and photochemistry. The nucleation-mode particles gradually shifted towards larger sizes at both stations; however, at Santorini the number of particles remained high for several hours, indicating regional NPF. During the MSF period, the total number concentration of the particles reached lower values, while nucleation-mode particles were not detected at any of the stations.

The observed NPF events were initiated at least 250 km (covered within 4.5 h) to the northeast of Santorini in the center of AS, upwind of the Cyclades complex, under favorable meteorological conditions, under a strong-channeled northeastern wind flow received by both stations. Based on the simulations, it seems that what contributed to the NPF events was the clean air masses of low preexisting aerosol particles with sufficient H_2SO_4 from high altitudes. In contrast to the non-NPF period, the air masses passed over the greater Istanbul area, avoiding mixing with the local emissions. Thereafter, they penetrated at lower levels (due to the EF structure) over northwestern Turkey, while in the case of the non-NPF period, they suffered a strong mixing during their longer journey over the Turkish mainland. Without excluding the role of photochemistry in NPF, we show by both measurements and simulations that the plume over AS moved fast with rather negligible mixing, especially above the MABL. The fast advection above MABL and the low number of preexisting concentrations inside the plume prevented the subsequent growth of the nucleated particles towards the central Aegean Sea. The wakes on the lee side of the islands, however, enhanced vertical mixing, enabling the plume's subsequent entrainment into the MABL in the central Aegean Sea. The freshly nucleated particles that remained constantly inside the well-mixed MABL suffered early aging (i.e., growth by condensation and coagulation).

To understand the impact of NPF on CCN levels, using the κ of particles in conjunction with a typical supersaturation for the area, we calculated the number concentration of particles that act as CCN at both stations. NPF was found to augment CCN concentrations considerably during early afternoon (87 % on average for both stations and both events), with concentration levels at Finokalia being higher due to particle growth and atmospheric processing. Calculations of droplet number generated in clouds within the observed air masses indicate that NPF augments droplet number, but to a much lesser extent (12 %) than implied by the variations in CCN. This behavior demonstrates that there is a limit to the amount of droplets that NPF can contribute because the supersaturation in clouds depresses (here, by roughly 14 %) as additional CCN are added by NPF. The pre-NPF aerosol levels and prevailing dynamics of the clouds determine the degree of water vapor competition and precondition cloud sensitivity – or lack thereof – to further CCN increases from NPF.

5 Data availability

Data are available upon request to the owners or to the principle investigator.

The Supplement related to this article is available online at doi:10.5194/acp-17-175-2017-supplement.

Acknowledgements. Athanasios Nenes acknowledges support from a Georgia Power Faculty Scholar Chair and a Cullen-Peck Faculty Fellowship. This work was supported by computational time granted from the Greek Research & Technology Network (GRNET) in the National HPC facility – ARIS.

Edited by: K. Lehtinen
Reviewed by: two anonymous referees

References

Ackermann, I. J., Hass, H., Memmesheimer, M., Ebel, A., Binkowski, F. S., and Shankar, U.: Modal Aerosol Dynamics model for Europe: Development and first applications, Atmos. Environ., 32, 2981–2999, 1998.

Anagnostopoulou, C., Zanis, P., Katragkou, E., Tegoulias, I., and Tolika, K.: Recent past and future patterns of the Etesian winds based on regional scale climate model simulations, Clim. Dynam., 42, 1819–1836, doi:10.1007/s00382-013-1936-0, 2014.

Barahona, D., West, R. E. L., Stier, P., Romakkaniemi, S., Kokkola, H., and Nenes, A.: Comprehensively accounting for the effect of giant CCN in cloud activation parameterizations, Atmos. Chem. Phys., 10, 2467–2473, doi:10.5194/acp-10-2467-2010, 2010.

Bardouki, H., Liakakou, H., Economou, C., Sciare, J., Smolìk, J., Ždìmal, V., Eleftheriadis, K., Lazaridis, M., Dye, C., and Mihalopoulos, N.: Chemical composition of size-resolved atmospheric aerosols in the eastern Mediterranean during summer and winter, Atmos. Environ., 37, 195–208, 2003.

Bezantakos, S., Barmpounis, K., Giamarelou, M., Bossioli, E., Tombrou, M., Mihalopoulos, N., Eleftheriadis, K., Kalogiros, J., D. Allan, J., Bacak, A., Percival, C. J., Coe, H., and Biskos, G.: Chemical composition and hygroscopic properties of aerosol particles over the Aegean Sea, Atmos. Chem. Phys., 13, 11595–11608, doi:10.5194/acp-13-11595-2013, 2013.

Binkowski, F. S. and Shankar, U.: The Regional Particulate Matter Model: 1. Model description and preliminary results, J. Geophys. Res., 100, 26191–26209, doi:10.1029/95JD02093, 1995.

Birmili, W., Berresheim, H., Plass-Dülmer, C., Elste, T., Gilge, S., Wiedensohler, A., and Uhrner, U.: The Hohenpeissenberg aerosol formation experiment (HAFEX): a long-term study including size-resolved aerosol, H_2SO_4, OH, and monoterpenes measurements, Atmos. Chem. Phys., 3, 361–376, doi:10.5194/acp-3-361-2003, 2003.

Bossioli, E., Tombrou, M., Kalogiros, J., Allan, J., Bacak, A., Bezantakos, S., Biskos, G., Coe, H., Jones, B. T., Kouvarakis, G., Mihalopoulos, N., and Percival, C. J.: Atmospheric composition

in the Eastern Mediterranean: Influence of biomass burning during summertime using the WRF-Chem model, Atmos. Environ., 132, 317–331, 2016.

Bougiatioti, A., Fountoukis, C., Kalivitis, N., Pandis, S. N., Nenes, A., and Mihalopoulos, N.: Cloud condensation nuclei measurements in the marine boundary layer of the Eastern Mediterranean: CCN closure and droplet growth kinetics, Atmos. Chem. Phys., 9, 7053–7066, doi:10.5194/acp-9-7053-2009, 2009.

Bougiatioti, A., Nenes, A., Fountoukis, C., Kalivitis, N., Pandis, S. N., and Mihalopoulos, N.: Size-resolved CCN distributions and activation kinetics of aged continental and marine aerosol, Atmos. Chem. Phys., 11, 8791–8808, doi:10.5194/acp-11-8791-2011, 2011.

Bougiatioti, A., Zarmpas, P., Koulouri, E., Antoniou, M., Theodosi, C., Kouvarakis, G., Saarikoski, S., Mäkelä, T., Hillamo, R., and Mihalopoulos, N.: Organic, elemental and water-soluble organic carbon in size segregated aerosols, in the marine boundary layer of the Eastern Mediterranean, Atmos. Environ., 64, 251–262, 2013.

Bougiatioti, A., Stavroulas, I., Kostenidou, E., Zarmpas, P., Theodosi, C., Kouvarakis, G., Canonaco, F., Prévôt, A. S. H., Nenes, A., Pandis, S. N., and Mihalopoulos, N.: Processing of biomass-burning aerosol in the eastern Mediterranean during summertime, Atmos. Chem. Phys., 14, 4793–4807, doi:10.5194/acp-14-4793-2014, 2014.

Boy, M. and Kulmala, M.: Nucleation events in the continental boundary layer: Influence of physical and meteorological parameters, Atmos. Chem. Phys., 2, 1–16, doi:10.5194/acp-2-1-2002, 2002.

Brody, L. R. and Nestor, M. J. R.: Regional forecasts for the Mediterranean basin, Technical Report, Naval Environmental Prediction Research Facility, Monterey, California, USA, no. 80–110, 1985.

Crippa, P. and Pryor, S. C.: Spatial and temporal scales of new particle formation events in eastern North America, Atmos. Environ., 75, 257–264, doi:10.1016/j.atmosenv.2013.04.051, 2013.

Crippa, P., Petäjä, T., Korhonen, H., El Afandi, G. S., and Pryor, S. C.: Evidence of an elevated source of nucleation based on model simulations and data from the NIFTy experiment, Atmos. Chem. Phys., 12, 8021–8036, doi:10.5194/acp-12-8021-2012, 2012.

Eleftheriadis, K., Colbeck, I., Housiadas, C., Lazaridis, M., Mihalopoulos, N., Mitsakou, C., Smolík, J., and Ždímal, V.: Size distribution, composition and origin of the submicron aerosol in the marine boundary layer during the eastern Mediterranean "SUB-AERO" experiment, Atmos. Environ., 40, 6245–6260, doi:10.1016/j.atmosenv.2006.03.059, 2006.

Formenti, P., Reiner, T., Sprung, D., Andreae, M. O., Wendisch, M., Wex, H., Kindred, D., Dewey, K., Kent, J., Tzortziou, M., Vasaras, A., and Zerefos, C.: STAAARTE-MED 1998 summer airborne measurements over the Aegean Sea 1., Aerosol particles and trace gases, J. Geophys. Res., 10, 4450, doi:10.1029/2001JD001337, 2002a.

Formenti, P., Boucher, O., Reiner, T., Sprung, D., Andreae, M. O., Wendisch, M., Wex, H., Kindred, D., Tzortziou, M., Vasaras, A., and Zerefos, C.: STAAARTE-MED 1998 summer airborne measurements over the Aegean Sea 2., Aerosol scattering and absorption, and radiative calculations, J. Geophys. Res., 107, 4451, doi:10.1029/2001JD001536, 2002b.

Gauss, M., Benedictow, A. C., Fagerli, H., and Steensen, B. M.: EMEP/MSC-W model performance for acidifying and eutrophying components and photo-oxidants in 2009, Supplementary material to EMEP Status Report 1/2011, METEOROLOGISK INSTITUTT, Norwegian Meteorological Institute, EMEP July, 2011.

Gerasopoulos, E., Kouvarakis, G., Vrekoussis, M., Kanakidou, M., and Mihalopoulos, N.: Ozone variability in the marine boundary layer of the eastern Mediterranean based on 7-year observations, J. Geophys. Res.-Atmos., 110, D15309, doi:10.1029/2005JD005991, 2005.

Gerasopoulos, E., Koulouri, E., Kalivitis, N., Kouvarakis, G., Saarikoski, S., Mäkelä, T., Hillamo, R., and Mihalopoulos, N.: Size-segregated mass distributions of aerosols over Eastern Mediterranean: seasonal variability and comparison with AERONET columnar size-distributions, Atmos. Chem. Phys., 7, 2551–2561, doi:10.5194/acp-7-2551-2007, 2007.

Ghan, S. J., Abdul-Razzak, H., Nenes, A., Ming, Y., Liu, X., Ovchinnikov, M., Shipway, B., Meskhidze, N., Xu, J., and Shi, X.: Droplet Nucleation: Physically-based Parameterization and Comparative Evaluation, J. Adv. Model. Earth Syst., 3, M10001, doi:10.1029/2011MS000074, 2011.

Grell, G. A., Peckham, S. E., Schmitz, R., McKeen, S. A., Frost, G., Skamarock W. C., and Eder, B.: Fully coupled "online" chemistry within the WRF model, Atmos. Environ., 39, 6957–6975, 2005.

Hodnebrog, Ø., Solberg, S., Stordal, F., Svendby, T. M., Simpson, D., Gauss, M., Hilboll, A., Pfister, G. G., Turquety, S., Richter, A., Burrows, J. P., and Denier van der Gon, H. A. C.: Impact of forest fires, biogenic emissions and high temperatures on the elevated Eastern Mediterranean ozone levels during the hot summer of 2007, Atmos. Chem. Phys., 12, 8727–8750, doi:10.5194/acp-12-8727-2012, 2012.

Hussein, T., Junninen, H., Tunved, P., Kristensson, A., Dal Maso, M., Riipinen, I., Aalto, P. P., Hansson, H.-C., Swietlicki, E., and Kulmala, M.: Time span and spatial scale of regional new particle formation events over Finland and Southern Sweden, Atmos. Chem. Phys., 9, 4699–4716, doi:10.5194/acp-9-4699-2009, 2009.

Im, U. and Kanakidou, M.: Impacts of East Mediterranean megacity emissions on air quality, Atmos. Chem. Phys., 12, 6335–6355, doi:10.5194/acp-12-6335-2012, 2012.

Im, U., Markakis, K., Poupkou, A., Melas, D., Unal, A., Gerasopoulos, E., Daskalakis, N., Kindap, T., and Kanakidou, M.: The impact of temperature changes on summer time ozone and its precursors in the Eastern Mediterranean, Atmos. Chem. Phys., 11, 3847–3864, doi:10.5194/acp-11-3847-2011, 2011.

Kalabokas, P. D., Volz-Thomas, A., Brioude, J., Thouret, V., Cammas, J.-P., and Repapis, C. C.: Vertical ozone measurements in the troposphere over the Eastern Mediterranean and comparison with Central Europe, Atmos. Chem. Phys., 7, 3783–3790, doi:10.5194/acp-7-3783-2007, 2007.

Kalabokas, P. D., Mihalopoulos, N., Ellul, R., Kleanthous, S., and Repapis, C. C.: An investigation of the meteorological and photochemical factors influencing the background rural and marine surface ozone levels in the Central and Eastern Mediterranean, Atmos. Environ., 42, 7894–7906, doi:10.1016/j.atmosenv.2008.07.009, 2008.

Kalabokas, P. D., Cammas, J.-P., Thouret, V., Volz-Thomas, A., Boulanger, D., and Repapis, C. C.: Examination of the atmospheric conditions associated with high and low summer ozone levels in the lower troposphere over the eastern Mediterranean, Atmos. Chem. Phys., 13, 10339–10352, doi:10.5194/acp-13-10339-2013, 2013.

Kalivitis, N., Birmili, W., Stock, M., Wehner, B., Massling, A., Wiedensohler, A., Gerasopoulos, E., and Mihalopoulos, N.: Particle size distributions in the Eastern Mediterranean troposphere, Atmos. Chem. Phys., 8, 6729–6738, doi:10.5194/acp-8-6729-2008, 2008.

Kalivitis, N., Kouvarakis G., Bougiatioti A., Stavroulas I., Wiedensohler A., and Mihalopoulos N.: Five-years of atmospheric aerosol number size distribution measurements in Eastern Mediterranean, Geophys. Res. Abstracts, 16, EGU2014-15860-1, 2014.

Kalivitis, N., Kerminen, V.-M., Kouvarakis, G., Stavroulas, I., Bougiatioti, A., Nenes, A., Manninen, H. E., Petäjä, T., Kulmala, M., and Mihalopoulos, N.: Atmospheric new particle formation as a source of CCN in the eastern Mediterranean marine boundary layer, Atmos. Chem. Phys., 15, 9203–9215, doi:10.5194/acp-15-9203-2015, 2015.

Kallos, G., Kotroni, V., Lagouvardos, K., Papadopoulos, A., Varinou, M., and Kakaliagou, O.: Temporal and spatial scales for transport and transformation processes in the Eastern Mediterranean, Proc. Of the 22nd NATO/CCMS Int. Tchn. Meeting on Air pollution Modelling and its Application, Clermont-Ferrand, France, 6–11 June, 1998.

Kallos, G., Astitha, M., Katsafados, P., and Spyrou, C.: Long-Range Transport of Anthropogenically and Naturally Produced Particulate Matter in the Mediterranean and North Atlantic: Current State of Knowledge, J. Appl. Meteorol. Climatol., 46, 1230–1251, doi:10.1175/JAM2530.1, 2007.

Kanakidou, M., Mihalopoulos, N., Kindap, T., Im, U., Vrekoussis, M., Gerasopoulos, E., Dermitzaki, E., Unal, A., Koçak, M., Markakis, K., Melas, D., Kouvarakis, G., Youssef, A. F., Richter, A., Hatzianastassiou, N., Hilboll, A., Ebojie, F., Wittrock, F., von Savigny, C., Burrows, J. P., Ladstaetter-Weissenmayer, A., and Moubasher, H.: Megacities as hot spots of air pollution in the East Mediterranean, Atmos. Environ., 45, 1223–1235, doi:10.1016/j.atmosenv.2010.11.048, 2011.

Karydis, V. A., Capps, S. L., Russell, A. G., and Nenes, A.: Adjoint sensitivity of global cloud droplet number to aerosol and dynamical parameters, Atmos. Chem. Phys., 12, 9041–9055, doi:10.5194/acp-12-9041-2012, 2012.

Koçak, M., Theodosi, C., Zarmpas, P., Im, U., Bougiatioti, A., Yenigun, O., and Mihalopoulos, N.: Particulate matter (PM_{10}) in Istanbul: Origin, source areas and potential impact on surrounding regions, Atmos. Environ., 45, 6891–6900, 2011.

Köhler, H.: The nucleus in the growth of hygroscopic droplets, Tsans. Faraday Soc., 32, 1152, 1936.

Kopanakis, I., Eleftheriadis, K., Mihalopoulos, N., Lydakis-Simantiris, N., Katsivela, E., Pentari, D., Zarmpas, P., and Lazaridis, M.: Physico-chemical characteristics of particulate matter in the Eastern Mediterranean, Atmos. Res., 106, 93–107, doi:10.1016/j.atmosres.2011.11.011, 2012.

Kopanakis, I., Chatoutsidou, S. E., Torseth, K., Glytsos, T., and Lazaridis, M.: Particle number size distribution in the eastern Mediterranean: Formation and growth rates of ultrafine airborne atmospheric particles, Atmos. Environ., 77, 790–802, doi:10.1016/j.atmosenv.2013.05.066, 2013.

Kotroni, V., Lagouvardos, K., and Lalas, D.: The effect of the island of Crete on the Etesian winds over the Aegean Sea, Q. J. Roy. Meteorol. Soc., 127, 1917–1937, doi:10.1002/qj.49712757604, 2001.

Koulouri, E., Saarikoski, S., Theodosi, C., Markaki, Z., Gerasopoulos, E., Kouvarakis, G., Mäkelä, T., Hillamo, R., and Mihalopoulos, N.: Chemical composition and sources of fine and coarse aerosol particles in the Eastern Mediterranean, Atmos. Environ., 42, 6542–6550, doi:10.1016/j.atmosenv.2008.04.010, 2008.

Kouvarakis, G., Doukelis, Y., Mihalopoulos, N., Rapsomanikis, S., Sciare, J., and Blumthaler, M.: Chemical, physical, and optical characterization of aerosols during PAUR II experiment, J. Geophys. Res., 107, 8141, doi:10.1029/2000JD000291, 2002.

Kulmala, M., Laaksonen, A., and Pirjola, L.: Parameterizations for sulfuric acid/water nucleation rates, J. Geophys. Res., 103, 8301–8307, doi:10.1029/97JD03718, 1998.

Kulmala, M., Kerminen, V.-M., Anttila, T., Laaksonen, A., and O'Dowd, C. D.: Organic aerosol formation via sulphate cluster activation, J. Geophys. Res., 109, D04205, doi:10.1029/2003JD003961, 2004.

Kulmala, M., Petäjä, T., Nieminen, T., Sipilä, M., Manninen, H.E., Lehtipalo, K., Dal Maso, M., Aalto, P., Junninen, H., Paasonen, P., Riipinen, I., Lehtinen, K.E.J., Laaksonen, A., and Kerminen, V.-M.: Measurement of the nucleation of atmospheric aerosol particles, Nat. Protocol., 7, 1651–1667, doi:10.1038/nprot.2012.091, 2012.

Lazaridis, M., Eleftheriadis, K., Smolik, J., Colbeck, I., Kallos, G., Drossinos, Y., Zdimal, V., Vecera, Z., Mihalopoulos, N., Mikuska, P., Bryant, C., Housiadas, C., Spyridaki, A., Astitha, M., and Havranek, V.: Dynamics of fine particles and photooxidants in the Eastern Mediterranean (SUB-AERO), Atmos. Environ., 40, 6214–6228, doi:10.1016/j.atmosenv.2005.06.050, 2006.

Lazaridis, M., Dzumbova, L., Kopanakis, I., Ondracek, J., Glytsos, T., Aleksandropoulou, V., Voulgarakis, A., Katsivela, E., Mihalopoulos, N., and Eleftheriadis, K.: PM10 and PM2.5 levels in the eastern Mediterranean (Akrotiri research station, Crete, Greece), Water Air Soil Pollut., 189, 85–101, doi:10.1007/s11270-007-9558-y, 2008.

Lehtinen, K. E. J. and Kulmala, M.: A model for particle formation and growth in the atmosphere with molecular resolution in size, Atmos. Chem. Phys., 3, 251–257, doi:10.5194/acp-3-251-2003, 2003.

Lelieveld, J., Berresheim, H., Borrmann, S., Crutzen, P. J., Dentener, F. J., Fischer, H., Feichter, J., Flatau, P. J., Heland, J., Holzinger, R., Korrmann, R., Lawrence, M. G., Levin, Z., Markowicz, K. M., Mihalopoulos, N., Minikin, A., Ramanathan, V., Reus, M. de, Roelofs, G. J., Scheeren, H. A., Sciare, J., Schlager, H., Schultz, M., Siegmund, P., Steil, B., Stephanou, E. G., Stier, P., Traub, M., Warneke, C., Williams, J., and Ziereis, H.: Global Air Pollution Crossroads over the Mediterranean, Science, 298, 794–799, doi:10.1126/science.1075457, 2002.

Liu, S. C., McKeen, S. A., Hsie, E.-Y., Lin, X., Kelly, K. K., Bradshaw, J. D., Sandholm, S. T., Browell, E. V., Gregory, G. L., Sachse, G. W., Bandy, A. R., Thornton, D. C., Blake, D. R., Rowland, F. S., Newell, R., Heikes, B. G., Singh, H., and Talbot, R. W.: Model study of tropospheric trace species distribu-

tions during PEM-West A, J. Geophys. Res., 101, 2073–2085, doi:10.1029/95JD02277, 1996.

Manninen, H. E., Nieminen, T., Asmi, E., Gagné, S., Häkkinen, S., Lehtipalo, K., Aalto, P., Vana, M., Mirme, A., Mirme, S., Hõrrak, U., Plass-Dülmer, C., Stange, G., Kiss, G., Hoffer, A., Töro, N., Moerman, M., Henzing, B., de Leeuw, G., Brinkenberg, M., Kouvarakis, G. N., Bougiatioti, A., Mihalopoulos, N., O'Dowd, C., Ceburnis, D., Arneth, A., Svenningsson, B., Swietlicki, E., Tarozzi, L., Decesari, S., Facchini, M. C., Birmili, W., Sonntag, A., Wiedensohler, A., Boulon, J., Sellegri, K., Laj, P., Gysel, M., Bukowiecki, N., Weingartner, E., Wehrle, G., Laaksonen, A., Hamed, A., Joutsensaari, J., Petäjä, T., Kerminen, V.-M., and Kulmala, M.: EUCAARI ion spectrometer measurements at 12 European sites – analysis of new particle formation events, Atmos. Chem. Phys., 10, 7907–7927, doi:10.5194/acp-10-7907-2010, 2010.

Meskhidze, N., A. Nenes, Conant, W. C., and Seinfeld, J. H.: Evaluation of a new Cloud Droplet Activation Parameterization with In Situ Data from CRYSTAL-FACE and CSTRIPE, J. Geophys. Res., 110, D16202, doi:10.1029/2004JD005703, 2005.

Mihalopoulos, N., Stephanou, E., Kanakidou, M., Pilitsidis, S., and Bousquet, P.: Tropospheric aerosol ionic composition in the Eastern Mediterranean region, Tellus B, 49, 314–326, 1997.

Morales Betancourt, R. and Nenes, A.: Droplet activation parameterization: the population-splitting concept revisited, Geosci. Model Dev., 7, 2345–2357, doi:10.5194/gmd-7-2345-2014, 2014.

Morales, R. and Nenes, A.: Characteristic updrafts for computing distribution-averaged cloud droplet number, autoconversion rate and effective radius, J. Geophys. Res., 115, D18220, doi:10.1029/2009JD013233, 2010.

Nenes, A. and Seinfeld, J. H.: Parameterization of cloud droplet formation in global climate models, J. Geophys. Res, 108, 4415, doi:10.1029/2002JD002911, 2003.

Ng, N. L., Herndon, S. C., Trimborn, A., Canagaratna, M. R., Croteau, P. L., Onasch, T. B., Sueper, D., Worsnop, D. R., Zhang, Q., Sun, Y. L., and Jayne, J. T.: An Aerosol Chemical Speciation Monitor (ACSM) for routine monitoring of the composition and mass concentrations of ambient aerosol, Aerosol Sci. Technol., 45, 770–784, doi:10.1080/02786826.2011.560211, 2011.

Paronis, D., Dulac, F., Chazette, P., Hamonou, E., and Liberti, G. L.: Aerosol optical thickness monitoring in the Mediterranean, J. Aerosol Sci., 29, S671–S672, 1998.

Peckham, S., Grell, G. A., McKeen, S. A., Barth, M., Pfister, G., Wiedinmyer, C., Fast, J. D., Gustafson, W. I., Zaveri, R., Easter, R. C., Barnard, J., Chapman, E., Hewson, M., Schmitz, R., Salzmann, M., and Freitas, S.: WRF/Chem Version 3.3 User's Guide, NOAA Technical Memo., 98 pp., 2011.

Petters, M. D. and Kreidenweis, S. M.: A single parameter representation of hygroscopic growth and cloud condensation nucleus activity, Atmos. Chem. Phys., 7, 1961–1971, doi:10.5194/acp-7-1961-2007, 2007.

Pikridas, M., Bougiatioti, A., Hildebrandt, L., Engelhart, G. J., Kostenidou, E., Mohr, C., Prévôt, A. S. H., Kouvarakis, G., Zarmpas, P., Burkhart, J. F., Lee, B.-H., Psichoudaki, M., Mihalopoulos, N., Pilinis, C., Stohl, A., Baltensperger, U., Kulmala, M., and Pandis, S. N.: The Finokalia Aerosol Measurement Experiment – 2008 (FAME-08): an overview, Atmos. Chem. Phys., 10, 6793–6806, doi:10.5194/acp-10-6793-2010, 2010.

Pikridas, M., Riipinen, I., Hildebrandt, L., Kostenidou, E., Manninen, H., Mihalopoulos, N., Kalivitis, N., Burkhart, J. F., Stohl, A., Kulmala, M., and Pandis, S. N.: New particle formation at a remote site in the eastern Mediterranean, J. Geophys. Res.-Atmos., 117, D12205, doi:10.1029/2012JD017570, 2012.

Querol, X., Pey, J., Pandolfi, M., Alastuey, A., Cusack, M., Pérez, N., Moreno, T., Viana, M., Mihalopoulos, N., Kallos, G., and Kleanthous, S.: African dust contributions to mean ambient PM_{10} mass-levels across the Mediterranean Basin, Atmos. Environ., 43, 4266–4277, doi:10.1016/j.atmosenv.2009.06.013, 2009.

Salisbury, G., Williams, J., Holzinger, R., Gros, V., Mihalopoulos, N., Vrekoussis, M., Sarda-Estève, R., Berresheim, H., von Kuhlmann, R., Lawrence, M., and Lelieveld, J.: Ground-based PTR-MS measurements of reactive organic compounds during the MINOS campaign in Crete, July–August 2001, Atmos. Chem. Phys., 3, 925–940, doi:10.5194/acp-3-925-2003, 2003.

Schell, B., Ackermann, I. J., Hass, H., Binkowski, F. S., and Ebel, A.: Modeling the formation of secondary organic aerosol within a comprehensive air quality model system, J. Geophys. Res.-Atmos., 106, 28275–28293, 2001.

Sciare, J., Bardouki, H., Moulin, C., and Mihalopoulos, N.: Aerosol sources and their contribution to the chemical composition of aerosols in the Eastern Mediterranean Sea during summertime, Atmos. Chem. Phys., 3, 291–302, doi:10.5194/acp-3-291-2003, 2003.

Sciare, J., Oikonomou, K., Favez, O., Liakakou, E., Markaki, Z., Cachier, H., and Mihalopoulos, N.: Long-term measurements of carbonaceous aerosols in the Eastern Mediterranean: evidence of long-range transport of biomass burning, Atmos. Chem. Phys., 8, 5551–5563, doi:10.5194/acp-8-5551-2008, 2008.

Seinfeld, J. and Pandis, S. (Eds.): Atmospheric Chemistry and Physics: From Air Pollution to Climate Change, 2nd Edn., John Wiley, edited by: Hoboken, N. J., ISBN: 978-0-471-72018-8, 1232 pp., 2006.

Stein, A. F., Draxler, R. R, Rolph, G. D., Stunder, B. J. B., Cohen, M. D., and Ngan, F.: NOAA's HYSPLIT atmospheric transport and dispersion modeling system, B. Am. Meteorol. Soc., 96, 2059–2077, doi:10.1175/BAMS-D-14-00110.1, 2015.

Stockwell, W. R., Middleton, P., Chang, J. S., and Tang, X.: The second generation regional acid deposition model chemical mechanism for regional air quality modeling. J. Geophys. Res.-Atmos., 95, 16343–16367, 1990.

Tombrou, M., Bossioli, E., Protonotariou, A. P., Flocas, H., Giannakopoulos, C., and Dandou, A.: Coupling GEOS-CHEM with a regional air pollution model for Greece, Atmos. Environ., 43, 4793–4804, doi:10.1016/j.atmosenv.2009.04.003, 2009.

Tombrou, M., Bossioli, E., Kalogiros, J., Allan, J. D., Bacak, A., Biskos, G., Coe, H., Dandou, A., Kouvarakis, G., Mihalopoulos, N., Percival, C. J., Protonotariou, A. P., and Szabó-Takács, B.: Physical and chemical processes of air masses in the Aegean Sea during Etesians: Aegean-GAME airborne campaign, Sci. Total Environ., 506–507, 201–216, doi:10.1016/j.scitotenv.2014.10.098, 2015.

Triantafyllou, E., Giamarelou, M., Bossioli, E., Zarmpas, P., Theodosi, C., Matsoukas, C., Tombrou, M., Mihalopoulos, N., and Biskos, G.: Particulate Pollution Transport Episodes from Eurasia to a Remote Region of Northeast Mediterranean, Atmos. Environ., 128, 45–52, doi:10.1016/j.atmosenv.2015.12.054, 2016.

Tuccella, P., Curci, G., Visconti, G., Bessagnet, B., Menut, L., and Park, R. J.: Modeling of gas and aerosol with WRF/Chem over Europe: evaluation and sensitivity study, J. Geophys. Res.-Atmos. 117, D03303, doi:10.1029/2011JD016302, 2012.

Tyrlis, E. and Lelieveld, J.: Climatology and Dynamics of the Summer Etesian Winds over the Eastern Mediterranean, J. Atmos. Sci., 70, 3374–3396, doi:10.1175/JAS-D-13-035.1, 2013.

Wiedensohler, A., Birmili, W., Nowak, A., Sonntag, A., Weinhold, K., Merkel, M., Wehner, B., Tuch, T., Pfeifer, S., Fiebig, M., Fjäraa, A. M., Asmi, E., Sellegri, K., Depuy, R., Venzac, H., Villani, P., Laj, P., Aalto, P., Ogren, J. A., Swietlicki, E., Williams, P., Roldin, P., Quincey, P., Hüglin, C., Fierz-Schmidhauser, R., Gysel, M., Weingartner, E., Riccobono, F., Santos, S., Grüning, C., Faloon, K., Beddows, D., Harrison, R., Monahan, C., Jennings, S. G., O'Dowd, C. D., Marinoni, A., Horn, H.-G., Keck, L., Jiang, J., Scheckman, J., McMurry, P. H., Deng, Z., Zhao, C. S., Moerman, M., Henzing, B., de Leeuw, G., Löschau, G., and Bastian, S.: Mobility particle size spectrometers: harmonization of technical standards and data structure to facilitate high quality long-term observations of atmospheric particle number size distributions, Atmos. Meas. Tech., 5, 657–685, doi:10.5194/amt-5-657-2012, 2012.

Ždímal, V., Smolík, J., Eleftheriadis, K., Wagner, Z., Housiadas, C., Mihalopoulos, N., Zbynek Vecera, P. M., Kopanakis, I., and Lazaridis, M.: Dynamics of Atmospheric Aerosol Number Size Distributions in the Eastern Mediterranean During the SUB-AERO Project, Water Air Soil Pollut., 214, 133–146, doi:10.1007/s11270-010-0410-4, 2010.

Zerefos, C. S., Kourtidis, K. A., Melas, D., Balis, D., Zanis, P., Katsaros, L., Mantis, H. T., Repapis, C., Isaksen, I., Sundet, J., Herman, J., Bhartia, P. K., and Calpini, B.: Photochemical activity and solar ultraviolet radiation (PAUR) modulation factors: an overview of the project, J. Geophys. Res., 107, 8134, doi:10.1029/2000JD000134, 2002.